Review

Effect of Composition and Thermal Treatments on Mechanical Properties and Applications of Quenching and Partitioning Steels

Michele Maria Tedesco [1,2], **Daniele De Caro** [1,2], **Paola Rizzi** [2] and **Marcello Baricco** [2,*]

1 Stellantis, Metals and Anticorrosion Department, Corso Settembrini 40, 10135 Turin, Italy; michelemaria.tedesco@crf.it (M.M.T.); daniele.decaro@stellantis.com (D.D.C.)
2 Chemistry Department and NIS-INSTM, University of Turin, Via Pietro Giuria 7, 10125 Turin, Italy; paola.rizzi@unito.it
* Correspondence: marcello.baricco@unito.it

Abstract: In this review, we compared nine different chemical compositions and several heat treatments applied on quenching and partitioning steels investigated in the literature. All of these parameters were correlated to the reported mechanical properties (e.g., yield, tensile strength, elongation and toughness). Sustainability and a circular economy approach for applications in the automotive sector were also considered, providing hints for lightweighting in the car industry and the next possible steps to improve the decarbonization of the steel industry.

Keywords: quenching and partitioning steel; chemical composition; thermal treatment; mechanical properties; steel sustainability

1. Introduction

Nowadays, the automotive industry is affected by radical changes, from powertrain electrification to new business model development such as mobile sharing, from connectivity to sustainability. For sustainability goals, in the framework of a circular economy, recycling and decreasing the raw material usage as well as the decarbonization of processes for the main original equipment manufacturers (OEMs) are open challenges, aiming to anticipate as much as possible the targets released by the European Commission. In fact, in 2050, European industries must have net-zero greenhouse gas emissions [1]. Key players in this transition are materials from polymers to metals. In fact, focusing attention onto the metal side, the steel use in cars is highly impactful. As an example, in a battery electric vehicles (BEV), the steel weight is around 50–60% of the total car weight distributed in the vehicle, as described in Figure 1 for a Fiat 500e vehicle.

Based on these considerations, it is clear that reducing the steel amount has an impact on the sustainability aspects, meaning that lower CO_2 is emitted to make the car, thanks to less material utilization, and increases the vehicle autonomy range due to the weight reduction. To make this possible, it is necessary to consider new steel families and innovative manufacturing processes, from stamping to assembly. In this complex and challenging scenario, steel makers are involved to develop and introduce new steels with high mechanical properties and, at the same time, good formability behavior. One of the best results of this innovation are the quenching and partitioning (Q&P) steels, which are able to combine all of the mentioned requirements. The scope of this review was to collect the Q&P grades reported in the literature as well as the grades available on the market, in order to highlight the different compositions and heat treatments known to produce such steels, with a particular focus on the aspects that could play a relevant role in the circular economy and sustainability.
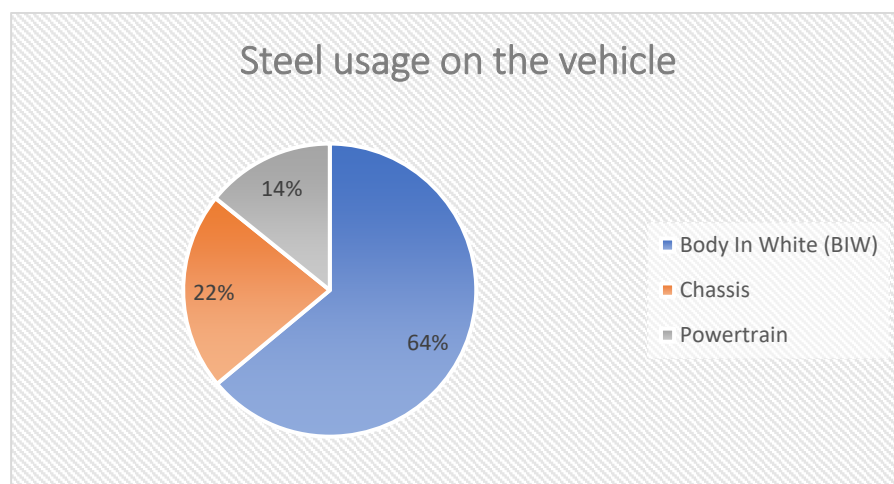
Figure 1. Steel distribution of the Fiat 500e vehicle subsystem perimeters.

2. Influence of Chemical Composition and Heat Treatment on Mechanical Properties

In 2003, Speer et al. [2] first proposed a new concept of advance high strength steels (AHSSs) containing retained austenite, which was the base for the development of the third steel generation. The idea behind this new steel family is the carbon diffusion from martensite into retained austenite for its stabilization, the so-called "quenching and partitioning" process, which is realized in two heating steps. During the first heating—the annealing—above the Ac_3 temperature, there is fully or partial steel austenization, followed by quenching with a cooling rate greater than 50 °C/s between the martensite start (Ms) and martensite finish (Mf) temperatures, which basically depends on the steel chemical composition [3,4]. At this stage, the microstructure of the steel is composed mainly of martensite and untransformed retained austenite (RA). The second step is isothermal holding at the quenching temperature and/or at a higher partition temperature, with the goal to enrich the RA with carbon, aiming to have this phase stable at room temperature after the last cooling of the material. In a typical steel, the supersaturated carbon in martensite would drive the precipitation of cementite, while the high silicon content of Q&P steel prevents the precipitation. The full thermal process for Q&P steels is presented in Figure 2. At the end of the process, the result is a microstructure with a matrix that consists mainly of tempered martensite, with a minor fraction of fresh martensite surrounded by metastable RA. Ferrite might also be present in the microstructure if the steel is annealed at the inter-critical temperature [4]. It is worth noting that the presence of ferrite in an inter-critical annealed steel results in a higher carbon content in the austenite (and in the primary martensite formed from it). This, in turn, affects the carbon partitioning process, thus modifying the morphology and improving the stability of the RA [5–7]. The prior austenitic grain size, the steel carbon content, and the grain size in the lath martensite structure have a great impact on the final mechanical properties of the steel.
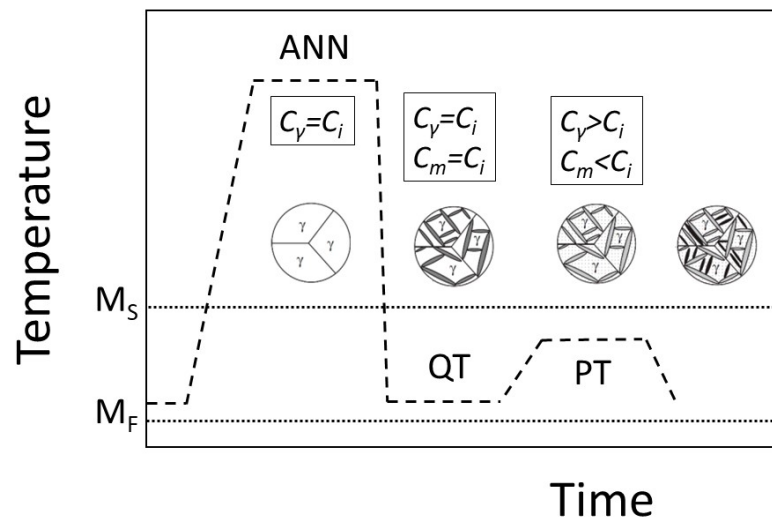
Figure 2. Thermal process to develop Q&P steels. ANN = annealing temperature; QT = quenching temperature; PT = partitioning temperature; M_S = martensite start temperature; M_F = martensite finish temperature. C_i, C_γ, and C_m are the carbon contents in the initial alloy, austenite, and martensite, respectively. Adapted from ref. [8].

Several studies and investigations have demonstrated that the Q&P process is able to provide steels with a good combination of tensile strength and formability, which are key aspects for automotive lightweighting. However, these characteristics are obtained only by adopting the most appropriate heat treatment and steel composition [4,7]. Tan et al. studied the contribution of RA in the strain hardening effect and found a correlation based on RA localization, morphology, and stability, which are essentially linked to the carbon-content in the steel [9]. If deformation occurs primarily in the ferrite phase, the transformation of retained austenite to martensite is limited, which reduces the total elongation of the steel. This means that alloying elements must be carefully selected to ensure successful quenching and partitioning (Q&P) processing.

First, for successful quenching and partitioning (Q&P) processing, the steel must be able to prevent or slow down the formation of carbides and other precipitates during the partitioning step. This is typically achieved by adding a combination of elements that stabilize ferrite such as aluminum, silicon, or chromium [10].

Adding small amounts of alloying elements such as aluminum (Al) and silicon (Si) to steel can change the rate of cementite formation from being controlled by carbon diffusion to being controlled by Si/Al diffusion [11]. This is because these elements have low solubility in cementite. However, care must be taken when adding Al and Si, as too much Al can increase the austenite finish temperature (Ac3), which can lead to undesirable austenite grain growth and reduce the strength and ductility [12]. Too much Si can also cause problems with coating the steel surface as it can form a Si-oxide (fayalite) layer that is difficult to remove. Additionally, a high Si content can reduce the weldability of the steel [13,14]. Some studies have shown that adding Nb to steel can also improve its strength by forming NbC precipitates during partitioning [15,16]. The Nb content may also indirectly influence the mechanical properties of Q&P steels by affecting the stability of retained austenite (RA) [17]. Several authors have studied the precipitation of the microalloying element in the quenching and partitioning process [16,18,19].

Second, the steel must contain a sufficient amount of carbon to enable the stabilization of an optimum RA fraction in order to achieve the desired increase in ductility.

Third, the steel must be also sufficiently hardenable to reach the initial quenching temperature without allowing for undesired ferritic or bainitic phase transformations during the initial cooling step [20].

In the literature, it is possible to observe a wide range of compositions for the Q&P steel grades. Nyyssönen et al. [20] tested three different compositions with a carbon content below 0.2 wt%. The steels were cast and rolled, and they could be hot dip galvanized in an industrial setting using existing technology. The annealing temperatures and times that were investigated were also chosen to be relevant to industrial applications. The Mn element can be alloyed to the steel in order to stabilize the RA, delaying the carbide precipitation during the bainitic transformation and promoting, during the plastic deformation, the transformation induced plasticity (TRIP) effect, where the RA transforms into martensite [21,22]. It is important to not exceed the Mn content to avoid the undesired segregation in the steel, which decreases the ferrite and initial martensite fractions during the inter-critical annealing and first quenching processes. The low ferritic microstructure fraction means less C available for partitioning, and thus a lower fraction and stability of the RA [23].

Y.Y. Cheng et al. [24] investigated the difference of hot rolled and cold rolled Q&P steels. The chemical composition of the tested steel was richer in carbon and silicon than those previously mentioned. To ensure a large volume fraction of RA, it is crucial to suppress carbide precipitation during the heat treatments. Due to the low solubility of Si in cementite, its precipitation during the partitioning step can be postponed, adding this alloying element in an adequate concentration [25]. Starting from the same carbon content (0.2%), the effect of Cr and Nb on Q&P steels has been also investigated [7]. Grain refinement is a way to make steel stronger and tougher. It can be achieved by thermomechanical processing or by adding micro-alloying elements such as niobium (Nb). NbC, a carbide that forms when Nb is added to steel, can refine grains, harden the steel, and affect hydrogen embrittlement (HE). Carbides and other precipitates can act as traps for hydrogen, which can reduce the amount of diffusible hydrogen, which is the main cause of ductility loss in HE [26,27]. The binding energy of the traps is important for HE sensitivity. Finely distributed, deep, irreversible traps are the most effective hydrogen trap sites because they lower the amount of diffusible hydrogen. On the other hand, traps with low binding energy (i.e., reversible trapping sites) can still release hydrogen, which can act as hydrogen sources during straining. The binding energy of NbC trapping sites ranges from 20 kJ/mol (weak) to 80 kJ/mol (deep) depending on the size, coherency with the matrix, and location of the traps (e.g., at the interface or inside the carbide) [28]. With Cr alloying, it is possible to have an austenitic phase stabilization on the material and then an improvement on the bending property [29]. It was also possible to observe steel compositions with high Mn content over 3%, the so-called "lean medium Mn Q&P steels", in the case investigated by Kaar et al. [25], where an increase up to 5 wt% of Mn contributed to a chemical stabilization of RA. In this research, the team evaluated the possibility to substitute the high Si content that promotes the formation of very strong oxide layers, which, after cold rolling, resulted in undesired galvanizing problems with Al. Nevertheless, it has to be considered that Al is less effective than Si in retarding the cementite precipitation, so the full substitution of these two elements showed a decrease in the strength–ductility relation.

The composition of considered Q&P steels, as reported by Nyyssönen et al. [20], Kaar et al. [25], Xia et al. [7], and Cheng et al. [24] are summarized in Table 1.

Beyond the chemical composition, another fundamental aspect to be considered to reach the expected mechanical properties of a Q&P steel is the thermal treatment. Considering the selected steels, it is possible to observe that the annealing, quenching, and partitioning temperatures changed for different compositions. In particular, the temperature investigated for the considered Q&P steel grades are reported in Table 2.

The selected temperatures were different from each other and, sometimes, steels with the same composition were subjected to different quenching temperatures. The grade I steels are highly interesting because several annealing temperatures on the same composition were tested to investigate the response to the treatment. For the partitioning step, the temperature was more uniform across the different studies. Most of the researchers selected the temperature of 400 °C, while for the low carbon steel with high Al (grades A, B,

and C), a higher temperature of 450 °C was selected. This parameter was designed for steels based on the Ms values measured in the dilatometry experiments and fitted martensitic transformation behavior [20].

Table 1. Chemical compositions (wt%) of the considered Q&P steels. Data were collected from Nyyssönen et al. [20], Kaar et al. [25], Xia et al. [7], and Cheng et al. [24].

Grade	C	Si	Mn	Al	Ni	Cr	Ti + Nb + V	Si + Cr + Mo	Other	Ref.
A	0.11	-	2.65	0.81	0.041	-	0.035	0.978	-	[20]
B	0.16	-	2.08	1.03	0.044	-	0.008	0.689	-	[20]
C	0.16	-	1.62	1.31	0.041	-	0.023	0.498	-	[20]
D	0.17	1.47	4.46	0.03	-	-	-	-	-	[25]
E	0.19	0.04	4.52	1.31	-	-	-	-	-	[25]
F	0.20	1.25	2.40	0.02	-	-	-	-	-	[7]
G	0.20	1.25	2.40	0.02	-	0.30	-	-	-	[7]
H	0.20	1.25	2.40	0.02	-	0.30	-	-	Nb (0.025)	[7]
I	0.21	1.69	1.94	-	-	-	-	-	P (0.008) S (0.0013) Ti (0.02) N (0.0039)	[24]

Table 2. Annealing, quenching, and partitioning temperatures applied to the considered Q&P steels grade. Data were collected from Nyyssönen et al. [20], Kaar et al. [25], Xia et al. [7], and Cheng et al. [24].

| Grade	Annealing (°C)	Quenching (°C)	Partitioning (°C)
A	850	200, 250, 275, 300	450
B	850	125, 150, 175	450
C	850	75, 100	450
D	900	130, 150, 170, 190, 210, 230, 250, 270, 290	400
E	900	130, 150, 170, 190, 210, 230, 250, 270, 290, 310, 330	400
F	870	300	400
G	870	280	400
H	870	290	400
I	780, 810, 840, 870	260	400

Taking into consideration steel grade I, it is possible to observe the effect of the annealing process on steel with the same composition. In fact, increasing the temperature from 780 °C to 870 °C but maintaining a constant quenching temperature of 260 °C and a partitioning temperature of 400 °C, a variation in the volume of the RA was observed, as shown in Figure 3. On raising the annealing temperature, after an increase in the RA fraction, it was possible to observe an inversion of this trend. This can be attributed to the fact that when the annealing temperature is increased, the volume fraction of ferrite decreases and that of austenite increases. During inter-critical annealing, carbon in the ferrite phase diffuses to the austenite phase, which improves the thermal stability of the austenite. If the annealing temperature is too low, less austenite will be formed, resulting in a lower retained austenite (RA) content in the Q&P steel. On the other hand, if the annealing temperature is too high, less ferrite will be formed, which means that the thermal stability of the austenite cannot be improved. As a result, more austenite with low thermal stability will be transformed into martensite during the first quenching, which also reduces the RA content in the Q&P steel. When the annealing temperature is increased to 870 °C, the carbon content of the RA increases. This is because a large amount of martensite is formed after quenching at this temperature. After carbon partitioning from the martensite laths, the carbon content of the untransformed austenite increases, which allows it to be retained at room temperature. In other words, the annealing temperature must be carefully controlled in order to achieve the desired RA content in the Q&P steel. Too low a temperature will

result in a lower RA content, while too high a temperature will also result in a lower RA content due to the transformation of austenite to martensite [24].
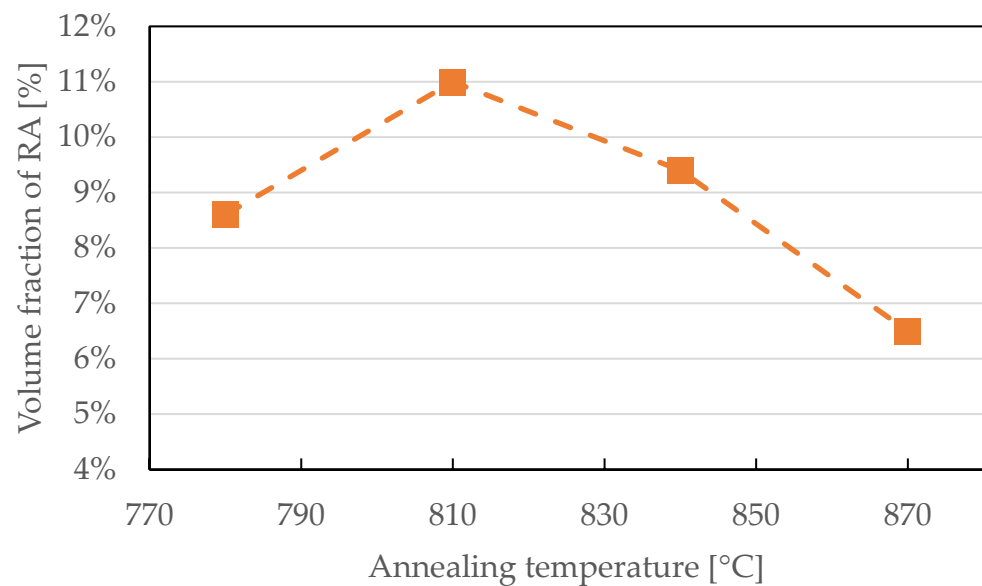
Figure 3. Effect of annealing temperature on RA of grade I Q&P steel; data from Cheng et al. [24].

Also, the quenching temperature had an important effect on the volume fraction of RA in the Q&P steels. In particular, it was possible to observe an increase in the RA content increasing the quenching temperature, up to certain value, but afterward, there was an inversion. The reversal temperature depends on the chemical composition of the steel. It was possible to observe this behavior when looking at the grade D and grade E Q&P steels, as reported in Figure 4. Both compositions were subjected to the same annealing, quenching, and partitioning temperatures, the only variable was the main alloying element, which was Si in the case of grade D and Al for grade E. For grades A, B, and C, only the RA fraction increase according to the increase in the quenching temperature was observed, as reported in Figure 4 for the three compositions quenched at different temperatures by Nyyssönen et al. [20].
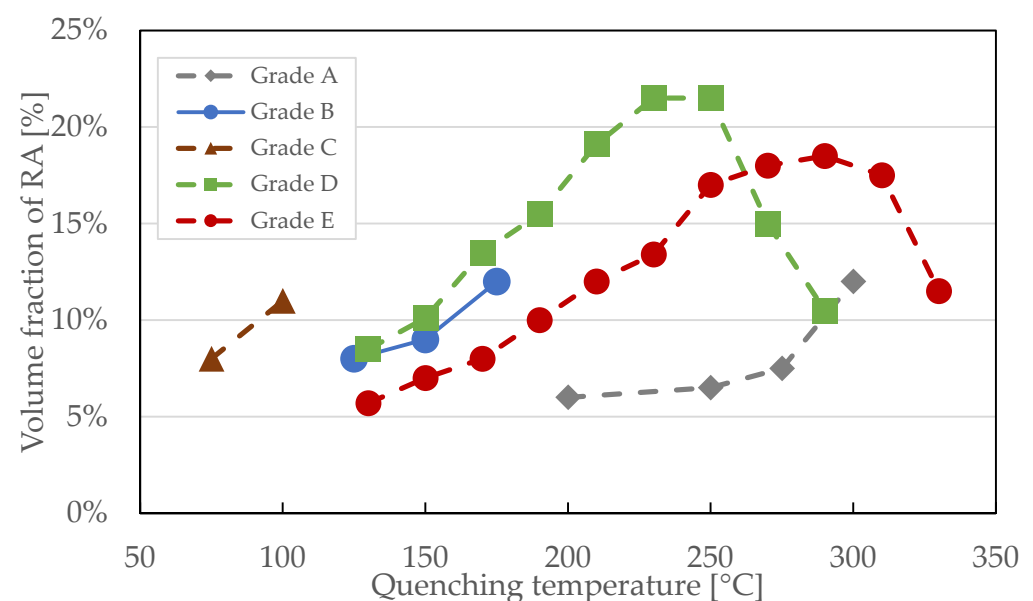
Figure 4. Effect of quenching temperature on the volume fraction of retained austenite for the considered Q&P steels. Data were collected from Nyyssönen et al. [20], Kaar et al. [25], Xia et al. [7], and Cheng et al. [24].

The quenching temperature also had an effect on the mechanical properties (i.e., yield strength, tensile strength, and elongation), which are obviously linked to the steel microstructure. The collected data are summarized in Figure 5.
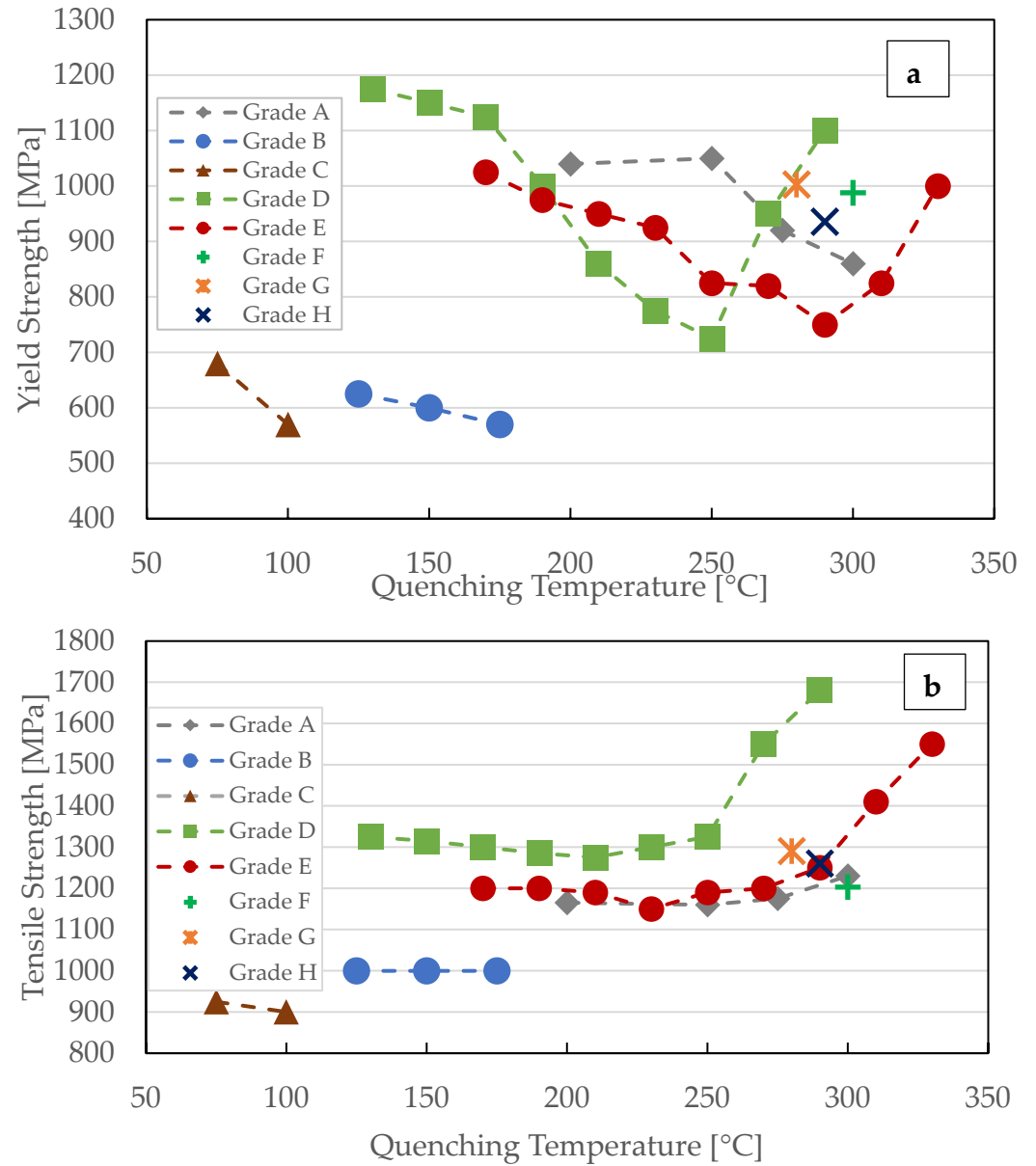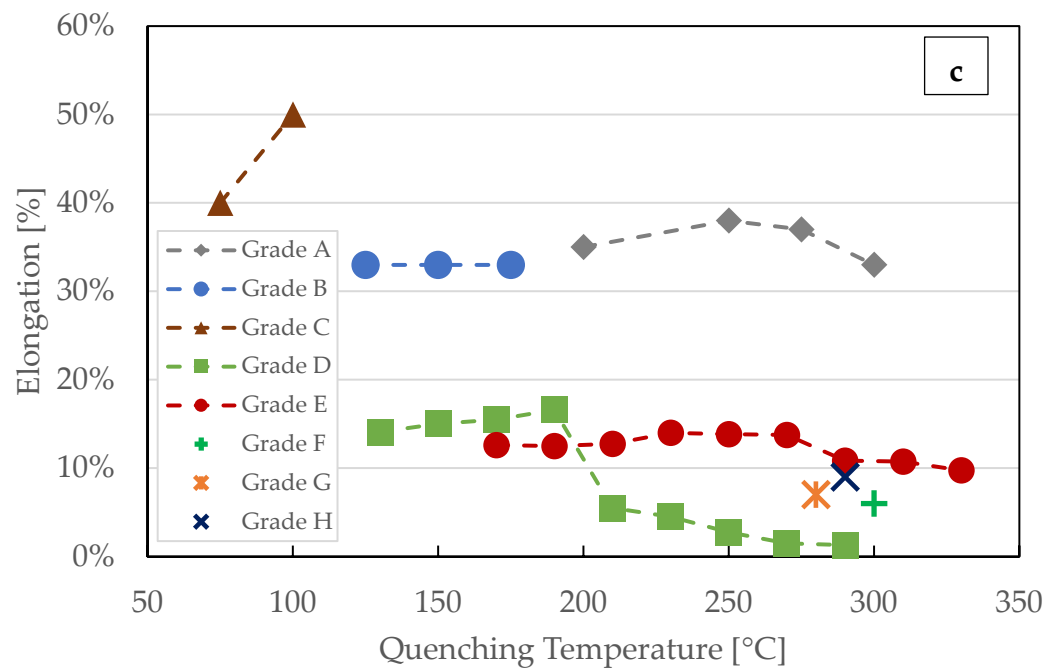

Figure 5. *Cont.*

Figure 5. Influence of quenching temperature in the thermal treatments of Q&P steels on: (**a**) yield strength; (**b**) tensile strength; (**c**) elongation. Data were collected from Nyyssönen et al. [20], Kaar et al. [25], Xia et al. [7], and Cheng et al. [24].

Considering the same steel composition, a decrease in yield stress was observed when increasing the quenching temperature, as shown in Figure 5a. An exception to this trend was given by the grade D and grade E Q&P steels for which, after the decrease in yield stress, there was an inversion, so that the yield point started to increase. The inversion point corresponded to the decrease in the fraction of RA, as shown in Figure 4, highlighting that the higher the volume fraction of RA, the lower the yield strength of the material. Steel with unstable austenite grains has a very high initial strain hardening rate. This means that it becomes much stronger as it is deformed, which results in a high ultimate tensile strength (UTS). However, it also has a low initial yield point, which means that it starts to deform at a relatively low stress. The tensile strength seems to be less sensitive than the yield point with respect to the quenching temperature variation, as shown in Figure 5b. In fact, the reported values were rather similar for most of the considered Q&P steels. Also in this case, the grade D and E Q&P steels showed a different trend after 250 °C, displaying a decrease in RA content and an increase in the tensile strength. It is interesting to compare grades A and E. In fact, despite the different chemical composition (i.e., different carbon content), they showed a similar trend in terms of the yield and tensile strength, in correlation with the quenching temperature. This kind of behavior could be justified by the Mn and Al contents, both being Q&P steels of grade A and E characterized by high Mn and Al contents.

The elongation value was less affected by the quenching temperature for almost all of the considered Q&P steels, as shown in Figure 5c. The only chemical composition that showed a different behavior was grade D, for which, after 200 °C, there was a more pronounced elongation decrease compared to the other steels. This behavior could be justified by the stability of RA under mechanical deformation. Mechanical deformation of the retained austenite (RA), which is metastable at room temperature, causes it to transform into martensite, resulting in the TRIP effect. An RA with intermediate stability is ideal for achieving the best combination of ultimate tensile strength (UTS) and elongation. Very high RA stability results in very low elongation due to an insufficient TRIP effect. Conversely, very unstable RA easily transforms into strain-induced primary martensite, resulting in an extremely high work hardening rate at the onset of straining, followed by a rapid drop during further deformation. The high carbon (C) content of the RA and the

presence of final martensite in the initial microstructure of grade D steel adversely affect the final stress–strain behavior. The strain-induced transformation of C-enriched RA to hard primary martensite causes volume expansion and increases the dislocation density, which hinders the undisturbed movement of dislocations during straining. This leads to premature failure prior to necking. In simpler terms, RA stability has a significant impact on the UTS and elongation of steel. An RA with intermediate stability is ideal for achieving the best combination of these properties. Very high or very low RA stability can lead to poor mechanical performance. The C content of the RA and the presence of final martensite in the initial microstructure can also have a negative impact on the stress–strain behavior of steel [25].

## 3. Mechanical Properties and Applications

Q&P steels are very strong and formable, making them ideal for use in car bodies. They are also very good at absorbing energy, which helps to protect occupants in the event of a crash. Q&P steels are also easy to shape, making them a versatile and high-performance material for automotive applications, for example, B pillars, cross members, and side sills [30]. A commercial cold rolled Q&P 980, where 980 MPa is the minimum requested tensile strength, has a total elongation of approximately 20%, and cold rolled Q&P 1180, with a minimum tensile strength of 1180 MPa, has a total elongation of approximately 12%. Figure 6 shows typical forming-limit curves for a cold rolled Q&P steel (QP980) compared with a traditional dual-phase AHSS (i.e., DP780 and DP980 [31,32], with a minimum tensile strength of 780 MPa and 980 MPa, respectively). The major strain describes the sample deformation along the vertical axis, according to the international standard ISO 12004-2, while the minor strain is the deformation along the horizontal one. The curve indicates the maximum steel deformation before the crack appearance, meaning that the higher the curve, the more formable the material. The formability of the QP 980 steel is definitely superior to that of the DP980 steel and it reaches values shown by DP780 [33,34].
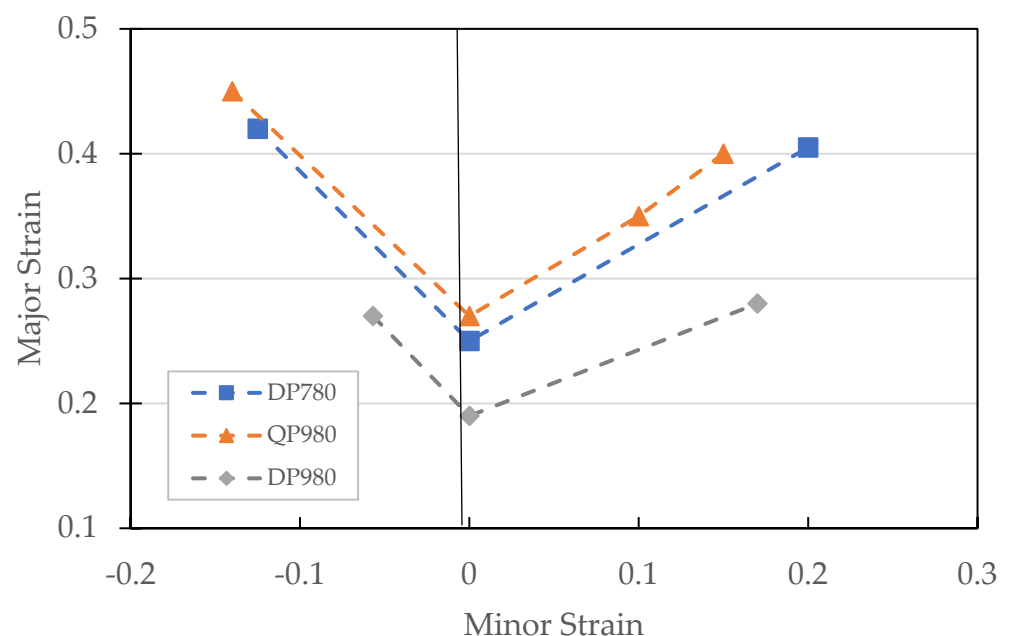
Figure 6. Forming–limit curve of a Q&P steel (QP980) compared to traditional AHSSs (DP780 and DP980) [31,32].

The superior properties of Q&P steels in comparison with conventional AHSSs is also shown in the so called "Banana diagram", where the tensile strength and the elongation (global formability) are plotted for the different steel families. The mechanical properties reported for the Q&P steels in Nyyssönen et al. [20], Kaar et al. [25], Xia et al. [7], and

Cheng et al. [24] (see Figure 5) are reported in Figure 7. For comparison, the tensile strength and elongation values, collected from the Stellantis cold forming steel standard, are also reported for various steels.
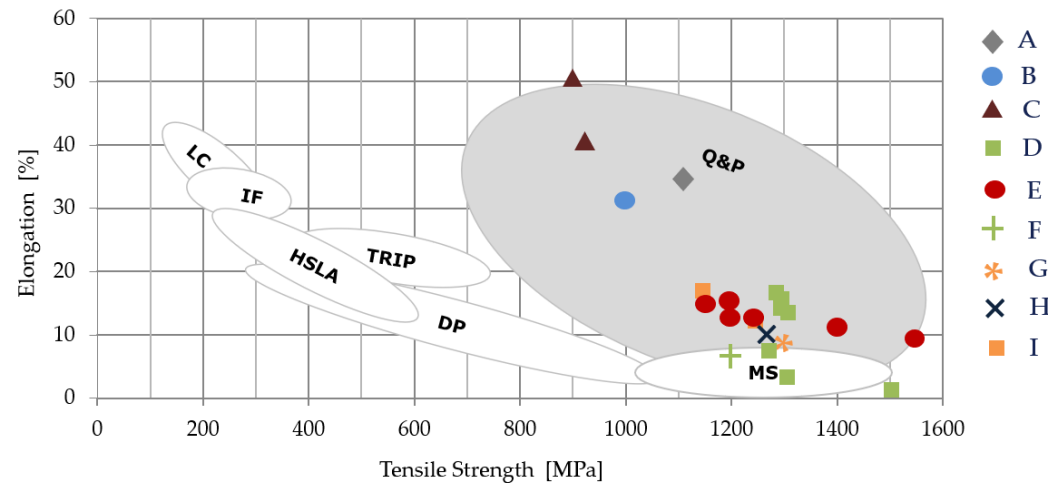
Figure 7. "Banana diagram" providing elongation vs. tensile strength for the considered Q&P steels. Data were collected from Nyyssönen et al. [20], Kaar et al. [25], Xia et al. [7], and Cheng et al. [24]. For comparison, values collected from the Stellantis cold forming steel standard are also reported: LC = low-carbon; IF = interstitial-free; HSLA = high-strength low-alloy; TRIP = transformation-induced-plasticity; DP = dual phase; MS = martensitic.

Edge formability is another mechanical characteristic that is important for automotive components. Several studies have demonstrated a correlation between this aspect and the material fracture toughness [35–41]. Takahashi et al. [35] found that the edge flangeability of hot rolled high strength steels is linearly correlated with their fracture toughness (We), as measured by the hole expansion ratio (HER), according to the ISO 16630 standard. Fontein et al. [40] observed that the HER of a cold rolled steel with different bainite contents increased with increasing crack propagation resistance, which was measured using fracture mechanics. Similar conclusions were reached by Casellas et al. [36], Yoon et al. [41], and Frómeta et al. [37–39], who proposed that We is the key property that governs the edge cracking resistance of advanced high strength steels (AHSSs). In simpler terms, the edge flangeability of high strength steels is directly related to their fracture toughness. This is because steels with a higher fracture toughness are more resistant to crack propagation, which can lead to edge cracking during flanging. Edge cracking is a major concern in the formation of high strength steels as it can lead to the formation of defects and premature failure of the component. Therefore, it is important to select a steel with a sufficiently high fracture toughness to ensure that edge cracking does not occur. The diagram proposed by Frometa et al. [39] that suggests that a correlation between We and UTS is reported in Figure 8. From this plot, it is possible to observe that the Q&P steels clearly returned a higher toughness than the dual phase steels. This is a key aspect for the forming operation in the case of edge flanging or stretch forming near cut blank areas. Good behavior was also possible to observe for press hardening steel (PHS), in which the toughness was very high, comparable with complex phase steel (CP), with an ultimate tensile strength around 1000 MPa, and decrease at the dual phase steel level for UTS between 1500 and 1800 MPa. For this family of steel, it is important to underline that the We is strongly dependent from the edge surface, and so therefore the cutting technology used to make the sample, or more in general, the component. The best solution is to use laser cutting because the edge surface presents less defects than hard cutting, and this enhances the essential work of the fracture of the material. The best steel families for the toughness are complex phase, CP, and twinning induced plasticity (TWIP). These materials are low sensitive to the different conditions of edge clearance and in general return high toughness, so are suitable to make

components in which the edge fracture is the main mechanism of rupture during the forming operation.
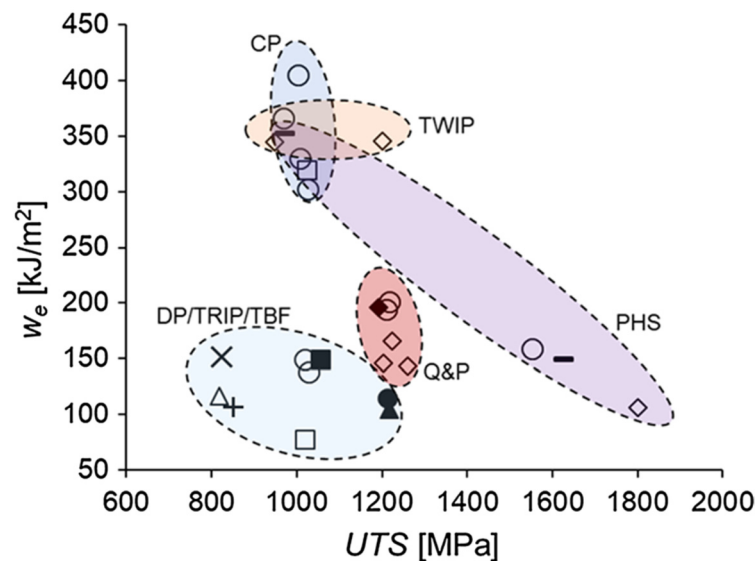
Figure 8. Frómeta plot reporting the fracture toughness (We) as a function of ultimate tensile strength (UTS). Values obtained for the Q&P steels were compared to those collected for different steels grades. Reprinted from ref. [39].

4. Sustainability

Today, there are two main routes to produce steel:

- The blast furnace/basic oxygen furnace (BF-BOF) process, which uses coke and coal as energy and reducing agents;
- The electric arc furnace (EAF) process by melting ferrous scraps.

A new technology is now under development, the direct reduced iron to EAF (DRI-EAF) technology, which has great potential to reduce energy consumption and the corresponding emissions. The DRI-EAF process uses hydrogen instead of coke to produce sponge iron and then feeds the iron into an EAF to produce crude steel. The CO_2 emissions of EAF are less than half compared to BF-BOF [42,43], and the particulate matter can be reduced by 89% [44]. BF-BOF, however, continues to dominate steel production, mainly in China, producing 88% of the total steel in 2022 [45]. To promote EAF technology, the first step is to maximize scrap collection, as it is assumed that ferrous scraps will increase, reaching a level sufficient to support 45% of the total crude-steel production in China in 2050 [46].

- Another way to decarbonize the steel mill industry is to implement the so-called carbon capture and storage (CCS) and carbon capture, utilization, and storage (CCUS) [47,48]; the latter is preferable because it is able to establish a circular economy approach [49].

For example, Valderrama et al. introduced the preparation of oxalic-acid- and glycolate-based polyester materials using CO_2 that can be taken from the steel industry [50], while Leflay et al. directly measured the ability of algae to capture CO_2 [51]. CCUS technology is the future in the development of low-carbon processes, nevertheless, today, there are a few applications, especially in China, that have not been taken into account yet [52,53].

It is likely that in the near future, CCS and CCUS implementation in the steel industry will be the basis of new research.

In terms of the sustainability of Q&P steels, an interesting study was reported by Goncalves et al. [54], who compared the different life cycle assessments (LCA) released on materials used for vehicle lightweighting. The study highlighted the AHSSs as the most preferable lightweight material, followed by aluminum alloys. The lower environmental

impact of AHSSs is related to a low energy-intensive production process and a high recycling rate (i.e., up to 80–95%). However, this study considered the same energy consumption and GHG emissions for AHSS production than for conventional steels. As a consequence of this assumption, a benefit toward the sustainability of AHSSs was obtained.

In order to maintain high quality in the chemical composition, the Q&P steels commercially available are nowadays basically produced by the BF-BOF metallurgical route. On the other hand, today, the main EAF plants use high scrap quality such as those delivered by the automotive sector, but are mixing them with poor scraps from the building sector, which are degrading their chemical composition. Nevertheless, it is still possible to improve the production routes of Q&P steels, in order to further decrease greenhouse gas (GHG) emissions.

Further studies and research are needed to find a way to produce them using the EAF, in order to mitigate the CO_2 emissions and promote a circular economy, decreasing the usage of primary raw material resources. As already mentioned, another way to reduce the CO_2 emissions for Q&P steels is to use the direct reduction iron (DRI) process, for which green hydrogen could be used to make sponge iron. This process, in comparison with the EAF, provides high quality chemical compositions, even better than the BF-BOF process, and could be the future of the steel industry.

5. Current Research Trend of Q&P Steels

Scientists are currently studying how the microstructure of Q&P steels changes during plastic deformation in order to predict their final mechanical properties. New techniques such as in situ SEM/EBSD-based tensile deformation and microscopic strain mapping have shown that the distribution of strain in Q&P steels is not uniform [55–58]. This is because Q&P steels are a mixture of soft and hard phases (fresh or tempered martensite) [59–61]. The amount of strain that is partitioned into each phase varies significantly, depending on the deformation behavior of the phase [62–64]. Several studies have shown that the local strain partitioned into the martensitic matrix determines whether the neighboring retained austenite (RA) transforms into martensite. There is also a wide variation in the local strain of RA, with some studies observing limited strain partitioning into RA and others observing a substantial amount of strain carried by RA in martensitic matrices [65–74]. In addition to strain partitioning, the microstructural strain path development also needs to be considered. Because several microstructural factors can compete depending on the thermomechanical history of the steel, it is still challenging to fully understand what controls the mechanical stability of RA in a given microstructure of a Q&P steel. The presence of multiple phases in different volumes and configurations further complicates this analysis and makes it difficult to systematically evaluate the individual effects. Similar challenges exist in understanding the behavior of mechanically-induced martensite, the transformed product from RA, relative to its neighboring stable phases. This is important to understand because mechanically-induced martensite plays a key role in the later stage of deformation, when ductile damage develops. Tailoring the neighborhood effects on both RA and other phases could be beneficial for improving the toughness of steels [75]. In simpler terms, scientists are trying to understand how the different phases in Q&P steels behave during plastic deformation. This information can be used to design Q&P steels with better mechanical properties. However, it is challenging to study the behavior of Q&P steels because they are made up of multiple phases with different properties. Other developments of Q&P steels are focused on the Mn additions. In fact, an increased Mn content allows for more RA at room temperature, leading to a higher formability and, at the same time, an enhancement in the strength [76]. However, ahigh Mn content (6–12 wt%) can have a negative effect on the strain rate sensitivity (SRS) of the steel. SRS is a measure of how the flow stress of a material changes with strain rate. Pure metals and most AHSSs have positive SRS, meaning that their flow stress increases with increasing strain rate [77]. However, some AHSSs such as TWIP steels and medium Mn steels have negative SRS [78–84]. This means that their flow stress decreases with an increasing strain

rate. There are four possible mechanisms that have been proposed to explain the negative SRS in AHSSs:

1. The Portevin–Le Chatelier (PLC) effect, or dynamic strain aging (DSA) effect. This effect is associated with pronounced serrations in the stress–strain curve of the steel [85–92].
2. Inhibition of martensitic transformation at a high strain rate. This can result in reduced TRIP hardening and negative SRS [93,94].
3. Suppression of dislocation multiplication, twinning, and martensitic transformation at a high strain rate due to adiabatic heating. Adiabatic heating is the heating of a material due to its deformation [95–98].
4. The newly formed martensite during high strain rate deformation is softer than that formed at a low strain rate. This can lead to a lower work hardening rate and negative SRS [99].

It is difficult to determine the underlying mechanisms of negative SRS in AHSSs because the deformation behavior of these steels is complex and involves multiple mechanisms; this is an interesting field of research to better predict the final Q&P mechanical properties during the crash event. In terms of sustainability and carbon dioxide emissions reduction, the main challenge is to produce AHSSs, and in particular Q&P steels, using EAF in combination with DRI, to allow for a decrease in greenhouse gases and, at the same time, create the possibility of increasing the recycling content in order to promote a circular economy approach, as mentioned in the previous section.

6. Conclusions

The different chemical composition and thermal treatments of Q&P steels were reviewed. In particular, their role on the base mechanical properties (yield, tensile strength, elongation and toughness) was highlighted. Finally, we briefly presented the GHG emission scenario for the steelmaking industry, especially for China, which is the first ranked producer in the world, suggesting possible approaches to reduce the environmental impacts for the Q&P steel industry.

The following conclusions can be drawn from the reported investigations:

- It is possible to produce Q&P steels with a specific microstructure, showing superior mechanical properties, by using alloy compositions that can be processed with the current level of technology.
- Q&P steels with different chemical compositions have to be processed by specific heat treatments, from annealing up to partitioning, in order to avoid too much RA volume fraction and, consequently, a low yield strength value. At the same time, it is fundamental to avoid a very stable RA, otherwise it returns a minor TRIP effect and therefore low ductility. Steel B has the most promising chemical composition in which changing the quenching temperature between 125 and 175 °C, the final behavior in terms of mechanical properties is also stable, showing high formability coupled with high tensile strength, which is needed for several automotive components.
- The AHSSs, and thus the Q&P steels, are the best sustainable choice for automotive lightweighting. Nevertheless, it is necessary to further improve the processing to be able to produce such steels using the EAF metallurgical route instead of BF-BOF, which is more polluting. For Q&P steel, probably the first step of decarbonization will be the implementation of CCUS that allows for the use of current blast furnace technology but can capture the emissions. The second step would be the implementation of EAF to produce this steel family by carefully controlling the scrap used and establishing a closed loop with the automotive industry, who are using high purity steels.
- A possible approach is the development of a closed loop between the automotive industry and EAF steelmakers, in order to return the stamping scraps to be re-melted and reused to produce origin grade Q&P steels, without a drop in the steel degrading. To do so, a specific and well-organized supply chain should be put in place to guarantee the correct flow of such processes.

References

1. European Environment Agency. Decarbonising Road Transport the Role of Vehicles. In *Fuels and Transport Demand*; Publications Office of the European Union: Luxembourg City, Luxemburg, 2022; ISBN 978-92-9480-473-0. [CrossRef]
2. Speer, J.; Matlock, D.K.; de Cooman, B.C.; Schroth, J.G. Carbon Partitioning into Austenite after Martensite Transformation. *Acta Mater.* **2003**, *51*, 2611–2622. [CrossRef]
3. Edmonds, D.V.; He, K.; Rizzo, F.C.; de Cooman, B.C.; Matlock, D.K.; Speer, J.G. Quenching and Partitioning Martensite-A Novel Steel Heat Treatment. *Mater. Sci. Eng. A* **2006**, *438–440*, 25–34. [CrossRef]
4. Moor, E.D.; Speer, J.G.; Matlock, D.K.; Kwak, J.-H.; Lee, S.-B. Effect of Carbon and Manganese on the Quenching and Partitioning Response of CMnSi Steels. *ISIJ Int.* **2011**, *51*, 137–144. [CrossRef]
5. Wang, X.; Liu, L.; Liu, R.D.; Huang, M.X. Benefits of intercritical annealing in quenching and partitioning steel. *Metall. Mater. Trans. A* **2018**, *49*, 1460–1464. [CrossRef]
6. Santofimia, M.J.; Zhao, L.; Sietsma, J. Overview of mechanisms involved during the quenching and partitioning process in steels. *Metall. Mater. Trans. A* **2011**, *42*, 3620–3626. [CrossRef]
7. Xia, P.; Vercruysse, F.; Celada-Casero, C.; Verleysen, P.; Petrov, R.; Sabirov, I.; Molina-Aldareguia, J.; Smith, A.; Linke, B.; Thiessen, R.; et al. Effect of Alloying and Microstructure on Formability of Advanced High-Strength Steels Processed via Quenching and Partitioning. *Mater. Sci. Eng. A* **2022**, *831*, 142217. [CrossRef]
8. Carpio, M.; Calvo, J.; García, O.; Pedraza, J.P.; Cabrera, J.M. Heat Treatment Design for a Qp Steel: Effect of Partitioning Temperature. *Metals* **2021**, *11*, 1136. [CrossRef]
9. Tan, X.; Ponge, D.; Lu, W.; Xu, Y.; Yang, X.; Rao, X.; Wu, D.; Raabe, D. Carbon and strain partitioning in a quenched and partitioned steel containing ferrite. *Acta Mater.* **2019**, *165*, 561–576. [CrossRef]
10. Jacques, P.; Girault, E.; Catlin, T.; Geerlofs, N.; Kop, T.; Van der Zwaag, S.; Delannay, F. Bainite Transformation of Low Carbon Mn-Si TRIP-Assisted Multiphase Steels: Influence of Silicon Content on Cementite Precipitation and Austenite Retention. *Mater. Sci. Eng. A* **1999**, *273–275*, 475–479. [CrossRef]
11. Clarke, A.J.; Speer, J.G.; Miller, M.K.; Hackenberg, R.E.; Edmonds, D.V.; Matlock, D.K.; Rizzo, F.C.; Clarke, K.D.; De Moor, E. Carbon partitioning to austenite from martensite or bainite during the quench and partition (Q&P) process: A critical assessment. *Acta Mater.* **2008**, *56*, 16–22. [CrossRef]
12. Traint, S.; Pichler, A.; Hauzenberger, K.; Stiaszny, P.; Werner, E. Influence of silicon, aluminium, phosphorus and copper on the phase transformations of low alloyed TRIP-steels. *Steel Res.* **2002**, *73*, 259–266. [CrossRef]
13. Song, E.J.; Suh, D.W.; Bhadeshia, H.K.D.H. Oxidation of silicon containing steel. *Ironmak. Steelmak.* **2012**, *39*, 599–604. [CrossRef]
14. Vercruysse, F.; Celada-Casero, C.; Linke, B.M.; Verleysen, P.; Petrov, R.H. The effect of Nb on the strain rate and temperature dependent behaviour of quenching & partitioning steels. *Mater. Sci. Eng.* **2021**, *800*, 140293. [CrossRef]
15. Zhang, J.; Ding, H.; Misra, R.D.K.; Wang, C. Microstructural evolution and consequent strengthening through niobium-microalloying in a low carbon quenched and partitioned steel. *Mater. Sci. Eng.* **2015**, *641*, 242–248. [CrossRef]
16. Wang, X.D.; Xu, W.Z.; Guo, Z.H.; Wang, L.; Rong, Y.H. Carbide characterization in a Nb-microalloyed advanced ultrahigh strength steel after quenching-partitioning-tempering process. *Mater. Sci. Eng.* **2010**, *527*, 3373–3378. [CrossRef]
17. Peng, F.; Xu, Y.; Gu, X.; Wang, Y.; Liu, X.; Li, J. The relationships of microstructure-mechanical properties in quenching and partitioning (Q&P) steel accompanied with microalloyed carbide precipitation. *Mater. Sci. Eng.* **2018**, *723*, 247–258. [CrossRef]
18. Zhou, S.; Zhang, K.; Wang, Y.; Gu, J.F.; Rong, Y.H. High strength-elongation product of Nb-microalloyed low-carbon steel by a novel quenching-partitioning-tempering process. *Mater. Sci. Eng.* **2011**, *528*, 8006–8012. [CrossRef]
19. Zhang, K.; Liu, P.; Li, W.; Guo, Z.; Rong, Y. Ultrahigh strength-ductility steel treated by a novel quenching-partitioning-tempering process. *Mater. Sci. Eng.* **2014**, *619*, 205–211. [CrossRef]
20. Nyyssönen, T.; Oja, O.; Jussila, P.; Saastamoinen, A.; Somani, M.; Peura, P. Quenching and Partitioning of Multiphase Aluminum-Added Steels. *Metals* **2019**, *9*, 373. [CrossRef]
21. Mishra, S.; Dalai, R.P. Effect of Quenching and Partitioning Treatment on Low Carbon Medium Manganese Alloyed Steels-A Short Review. *Mater. Today Proc.* **2020**, *43*, 593–596. [CrossRef]
22. Di Schino, A.; Emilio Di Nunzio, P.; Maria Cabrera, J. Effect of Quenching & Partitioning Process on a Low Carbon Steel. *Adv. Mater. Lett.* **2017**, *8*, 641–644. [CrossRef]

23. Wang, J.; Qian, R.; Yang, X.; Zhong, Y.; Shang, C. Effect of segregation on the microstructure and properties of a quenching and partitioning steel. *Mater. Lett.* **2022**, *325*, 132815. [CrossRef]
24. Cheng, Y.Y.; Zhao, G.; Xu, D.M.; Mao, X.P.; Bao, S.Q.; Yang, G.W. Comparative Study on Microstructures and Mechanical Properties of Q&P Steels Prepared with Hot-Rolled and Cold-Rolled C–Si–Mn Sheets. *J. Mater. Res. Technol.* **2022**, *20*, 1226–1242. [CrossRef]
25. Kaar, S.; Krizan, D.; Schneider, R.; Sommitsch, C. Impact of Si and Al on Microstructural Evolution and Mechanical Properties of Lean Medium Manganese Quenching and Partitioning Steels. *Steel Res. Int.* **2020**, *91*, 2000181. [CrossRef]
26. Du, Y.; Gao, X.; Lan, L.; Qi, X.; Wu, H.; Du, L.; Misra, R.D.K. Hydrogen Embrittlement Behavior of High Strength Low Carbon Medium Manganese Steel under Different Heat Treatments. *Int. J. Hydrogen Energy* **2019**, *44*, 32292–32306. [CrossRef]
27. Yang, J.; Huang, F.; Guo, Z.; Rong, Y.; Chen, N. Effect of Retained Austenite on the Hydrogen Embrittlement of a Medium Carbon Quenching and Partitioning Steel with Refined Microstructure. *Mater. Sci. Eng.* **2016**, *665*, 76–85. [CrossRef]
28. Vercruysse, F.; Claeys, L.; Depover, T.; Verleysen, P.; Petrov, R.H.; Verbeken, K. The Effect of Nb on the Hydrogen Embrittlement Susceptibility of Q&P Steel under Static and Dynamic Loading. *Mater. Sci. Eng.* **2022**, *852*, 143652. [CrossRef]
29. Ding, W.; Gong, Y.; Lu, Q.; Wang, J.; Wang, Z.; Li, W.; Jin, X. Improve Bendability of a Cr-Alloyed Press-Hardening Steel through an in-Line Quenching and Non-Isothermal Partitioning Process. *J. Manuf. Process.* **2022**, *84*, 481–493. [CrossRef]
30. Bouaziz, O.; Zurob, H.; Huang, M. Driving force and logic of development of advanced high strength steels for automotive applications. *Steel Res. Int.* **2013**, *84*, 937–947. [CrossRef]
31. Pierman, A.-P.; Bouaziz, O.; Pardoen, T.; Jacques, P.; Brassart, L. The influence of microstructure and composition on the plastic behaviour of dual-phase steels. *Acta Mater.* **2014**, *73*, 298–311. [CrossRef]
32. Wu-rong, W.; Chang-wei, H.; Zhong-hua, Z.; Xi-cheng, W. The limit drawing ratio and formability prediction of advanced high strength dual-phase steels. *Mater. Des.* **2011**, *32*, 3320–3327. [CrossRef]
33. Wang, L.; Speer, J.G. Quenching and Partitioning Steel Heat Treatment. *Metallogr. Microstruct. Anal.* **2013**, *2*, 268–281. [CrossRef]
34. Schwindta, C.D.; Stoutb, M.; Iurmana, L.; Signorelli, J.W. Forming Limit Curve Determination of a DP-780 Steel Sheet. *Procedia Mater. Sci.* **2015**, *8*, 978–985. [CrossRef]
35. Takahashi, Y.; Kawano, O.; Tanaka, Y. Fracture Mechanical Study on Edge Flange-ability of High Tensile-strength Steel Sheets. In Proceedings of the Materials Science & Technology Conference, Pittsburgh, PA, USA, 25–29 October 2009.
36. Casellas, D.; Lara, A.; Frómeta, D.; Gutiérrez, D.; Molas, S.; Pérez, L.; Rehrl, J.; Suppan, C. Fracture Toughness to Understand Stretch-Flangeability and Edge Cracking Resistance in AHSS. *Metall. Mater. Trans.* **2017**, *48*, 86–94. [CrossRef]
37. Frómeta, D.; Tedesco, M.M.; Calvo, J.; Lara, A.; Molas, S.; Casellas, D. Assessing edge cracking resistance in AHSS automotive parts by the Essential Work of Fracture methodology. *J. Phys. Conf. Ser.* **2017**, *896*, 012102. [CrossRef]
38. Frómeta, D.; Lara, A.; Parareda, S.; Casellas, D. Evaluation of Edge Formability in High Strength Sheets Through a Fracture Mechanics Approach. In Proceedings of the AIP Conference, Vitoria-Gasteiz, Spain, 8–10 May 2019.
39. Frómeta, D.; Lara, A.; Grifé, L.; Dieudonné, T.; Dietsch, P.; Rehrl, J.; Suppan, C.; Casellas, D.; Calvo, J. Fracture resistance of advanced high strength steel sheets for automotive applications. *Metall. Mater. Trans.* **2021**, *52*, 840–856. [CrossRef]
40. Fonstein, N.; Jun, H.J.; Huang, G.; Sriram, S.; Yan, B. Effect of Bainite on Mechanical Properties of Multiphase Ferrite-Bainite-Martensite Steels. In Proceedings of the Materials Science & Technology Conference, Columbus, OH, USA, 16–20 October 2011.
41. Yoon, J.I.; Jung, J.; Joo, S.H.; Song, T.J.; Chin, K.G.; Seo, M.H.; Kim, S.J.; Lee, S.; Kim, H.S. Correlation between fracture toughness and stretch-flangeability of advanced high strength steels. *Matter. Lett.* **2016**, *180*, 322–326. [CrossRef]
42. Hasanbeigi, A.; Jiang, Z.; Price, L. Retrospective and prospective analysis of the trends of energy use in Chinese iron and steel industry. *J. Clean. Prod.* **2014**, *74*, 105–118. [CrossRef]
43. Morfeldt, J.; Nijs, W.; Silveira, S. The impact of climate targets on future steel production–an analysis based on a global energy system model. *J. Clean. Prod.* **2015**, *103*, 469–482. [CrossRef]
44. Xuan, Y.; Yue, Q. Scenario analysis on resource and environmental benefits of imported steel scrap for China's steel industry. *Resour. Conserv. Recycl.* **2017**, *120*, 186–198. [CrossRef]
45. World Steel Association, 2022. World Steel in Figures 2022. Available online: https://worldsteel.org/steel-topics/statistics/world-steel-in-figures-2022/ (accessed on 31 August 2023).
46. Li, Z.; Hanaoka, T. Plant-Level Mitigation Strategies Could Enable Carbon Neutrality by 2060 and Reduce Non-CO_2 Emissions in China's Iron and Steel Sector. *One Earth* **2022**, *5*, 932–943. [CrossRef]
47. Cariou, P.; Parola, F.; Notteboom, T. Towards low carbon global supply chains: A multi-trade analysis of CO_2 emission reductions in container shipping. *Int. J. Prod. Econ.* **2019**, *208*, 17–28. [CrossRef]
48. Mersin, K.; Bayirhan, I.; Gazioglu, C. Review of CO_2 emission and reducing methods. *Therm. Sci.* **2019**, *23*, 2073–2078. [CrossRef]
49. Nocito, F.; Dibenedetto, A. Atmospheric CO_2 mitigation technologies: Carbon capture utilization and storage (CCUS). *Curr. Opin. Green Sust.* **2019**, *19*, 34–43. [CrossRef]
50. Valderrama, M.A.; Putten, R.J.; Gruter, G.M. The potential of oxalic—And glycolic acid based polyesters (review). Towards CO_2 as a feedstock (Carbon Capture and Utilization—CCU). *Eur. Polym. J.* **2019**, *119*, 445–468. [CrossRef]
51. Leflay, H.; Pandhal, J.; Brown, S. Direct measurements of CO_2 capture are essential to assess the technical and economic potential of algal-CCUS. *J. CO_2 Util.* **2021**, *52*, 101657. [CrossRef]
52. Global CCS Institute, 2020. The Global Status of CCS 2020. Available online: https://www.globalccsinstitute.com/wp-content/uploads/2021/03/Global-Status-of-CCS-Report-English.pdf (accessed on 31 August 2023).

53. Karali, N.; Xu, T.; Sathaye, J. Developing long-term strategies to reduce energy use and CO_2 emissions-analysis of three mitigation scenarios for iron and steel production in China. *Mitig. Adapt. Strat. Gl.* **2016**, *21*, 699–719. [CrossRef]

54. Gonçalves, M.; Monteiro, H.; Iten, M. Life Cycle Assessment Studies on Lightweight Materials for Automotive Applications—An Overview. *Energy Rep.* **2022**, *8*, 338–345. [CrossRef]

55. Yan, D.; Tasan, C.C.; Raabe, D. High resolution in situ mapping of microstrain and microstructure evolution reveals damage resistance criteria in dual phase steels. *Acta Mater.* **2015**, *96*, 399–409. [CrossRef]

56. Tasan, C.; Diehl, M.; Yan, D.; Zambaldi, C.; Shanthraj, P.; Roters, F.; Raabe, D. Integrated experimental–simulation analysis of stress and strain partitioning in multiphase alloys. *Acta Mater.* **2014**, *81*, 386–400. [CrossRef]

57. Stinville, J.C.; Vanderesse, N.; Bridier, F.; Bocher, P.; Pollock, T.M. High resolution mapping of strain localization near twin boundaries in a nickel-based superalloy. *Acta Mater.* **2015**, *98*, 29–42. [CrossRef]

58. Wei, S.; Kim, J.; Cann, J.L.; Gholizadeh, R.; Tsuji, N.; Tasan, C.C. Plastic straininduced sequential martensitic transformation. *Scr. Mater.* **2020**, *185*, 36–41. [CrossRef]

59. Wang, X.D.; Huang, B.X.; Rong, Y.H.; Wang, L. Microstructures and stability of retained austenite in TRIP steels. *Mater. Sci. Eng.* **2006**, *438–440*, 300–305. [CrossRef]

60. Xiong, Z.; Saleh, A.A.; Casillas, G.; Cui, S.; Pereloma, E.V. Phase-specific properties in a low-alloyed TRIP steel investigated using correlative nanoindentation measurements and electron microscopy. *J. Mater. Sci.* **2020**, *55*, 2578–2587. [CrossRef]

61. He, B.B.; Pan, S. Revealing the intrinsic nanohardness of retained austenite grain in a medium Mn steel with heterogeneous structure. *Mater. Charact.* **2021**, *171*, 110745. [CrossRef]

62. Tomota, Y.; Kuroki, K.; Mori, T.; Tamura, I. Tensile deformation of two-ductilephase alloys: Flow curves of α-γ Fe-Cr-Ni alloys. *Mater. Sci. Eng.* **1976**, *24*, 85–94. [CrossRef]

63. Furnémont, Q.; Lacroix, G.; Godet, S.; Conlon, K.; Jacques, P. Critical assessment of the micromechanical behaviour of dual phase and trip-assisted multiphase steels. *Can. Metall. Q.* **2004**, *43*, 35–42. [CrossRef]

64. De Diego-Calderón, I.; Santofimia, M.J.; Molina-Aldareguia, J.M.; Monclús, M.A.; Sabirov, I. Deformation behavior of a high strength multiphase steel at macroand micro-scales. *Mater. Sci. Eng.* **2014**, *11*, 201–211. [CrossRef]

65. Ryu, J.H.; Kim, D.I.; Kim, H.S.; Bhadeshia, H.K.; Suh, D.W. Strain partitioning and mechanical stability of retained austenite. *Scr. Mater.* **2010**, *63*, 297–299. [CrossRef]

66. Zhao, H.S.; Li, W.; Zhu, X.; Lu, X.H.; Wang, L.; Zhou, S.; Jin, X.J. Analysis of the relationship between retained austenite locations and the deformation behavior of quenching and partitioning treated steels. *Mater. Sci. Eng.* **2016**, *649*, 18–26. [CrossRef]

67. Long, X.; Zhang, R.; Zhang, F.; Du, G.; Zhao, X. Study on quasi-in-situ tensile deformation behavior in medium-carbon carbide-free bainitic steel. *Mater. Sci. Eng.* **2019**, *760*, 158–164. [CrossRef]

68. Koga, N.; Yamashita, T.; Umezawa, O. Strain distribution and deformationinduced martensitic transformation in tension for a TRIP steel plate. *ISIJ Int.* **2020**, *60*, 2083–2089. [CrossRef]

69. Zhao, F.; Chen, P.; Xu, B.; Yu, Q.; Misra, R.D.K.; Wang, G.; Yi, H. Martensite transformation of retained austenite with diverse stability and strain partitioning during tensile deformation of a carbide-free Bainitic steel. *Mater. Charact.* **2021**, *179*, 111327. [CrossRef]

70. Tan, X.; Ponge, D.; Lu, W.; Xu, Y.; He, H.; Yan, J.; Wu, D.; Raabe, D. Joint investigation of strain partitioning and chemical partitioning in ferrite-containing TRIP-assisted steels. *Acta Mater.* **2020**, *186*, 374–388. [CrossRef]

71. Li, Y.; Wang, M.; Huang, M. In-situ measurement of plastic strain in martensite matrix induced by austenite-to-martensite transformation. *Mater. Sci. Eng.* **2021**, *811*, 141061. [CrossRef]

72. Salehiyan, D.; Samei, J.; Amirkhiz, B.S.; Hector, L.G.; Wilkinson, D.S. Microstructural evolution during deformation of a QP980 steel. *Metall. Mater. Trans.* **2020**, *51*, 4524–4539. [CrossRef]

73. Wang, M.M.; Hell, J.C.; Tasan, C.C. Martensite size effects on damage in quenching and partitioning steels. *Scr. Mater.* **2017**, *138*, 1–5. [CrossRef]

74. Oh, H.S.; Biggs, K.; Güvenç, O.; Ghassemi-Armaki, H.; Pottore, N.; Tasan, C.C. In-situ investigation of strain partitioning and microstructural strain path development up to and beyond necking. *Acta Mater.* **2021**, *215*, 117023. [CrossRef]

75. Kang, J.; Pottore, N.S.; Zhu, H.; Tasan, C.C. An in situ investigation of neighborhood effects in a ferrite-containing quenching and partitioning steel: Mechanical stability, strain partitioning, and damage. *Acta Mater.* **2023**, *254*, 118985. [CrossRef]

76. Yang, H.; Liu, X. Study on the organization and properties of medium-Mn steel with V. In Proceedings of the MATEC Web of Conferences, Tianjin, China, 19 May 2022; Volume 358. [CrossRef]

77. Gray III, G.T. High-strain-rate deformation: Mechanical behavior and deformation substructures induced. *Annu. Rev. Mater. Res.* **2012**, *42*, 285–303. [CrossRef]

78. De Cooman, B.; Chen, L.; Kim, H.S.; Estrin, Y.; Kim, S.; Voswinckel, H. State-of-the-science of high manganese TWIP steels for automotive applications. In *Microstructure and Texture in Steels*; Springer: Berlin/Heidelberg, Germany, 2009; pp. 165–183. [CrossRef]

79. Zavattieri, P.; Savic, V.; Hector Jr., L.; Fekete, J.; Tong, W.; Xuan, Y. Spatio-temporal characteristics of the Portevin–Le Ĉhatelier effect in austenic steel with twinning induced plasticity. *Int. J. Plast.* **2009**, *25*, 2298–2330. [CrossRef]

80. Renard, K.; Ryelandt, S.; Jacques, P. Characterisation of the Portevin-Le Ĉhatelier effect affecting an austenitic TWIP steel based on digital image correlation. *Mater. Sci. Eng.* **2010**, *527*, 2969–2977. [CrossRef]

81. Alturk, R.; Hector, L.G.; Matthew Enloe, C.; Abu-Farha, F.; Brown, T.W. Strain rate effect on tensile flow behavior and anisotropy of a medium-manganese TRIP steel. *JOM* **2018**, *70*, 894–905. [CrossRef]

82. Callahan, M.; Perlade, A.; Schmitt, J.H. Interactions of negative strain rate sensitivity, martensite transformation, and dynamic strain aging in 3rd generation advanced high-strength steels. *Mater. Sci. Eng.* **2019**, *754*, 140–151. [CrossRef]

83. Cai, Z.; Zhang, D.; Ma, L.; Ding, H.; Feng, Y.; Hu, J.; Misra, R. Competing deformation mechanisms in an austenite-ferrite medium-Mn steel at different strain rates. *Mater. Sci. Eng.* **2021**, *818*, 141357. [CrossRef]

84. Wang, M.; Huang, M.X. Abnormal TRIP effect on the work hardening behavior of a quenching and partitioning steel at high strain rate. *Acta Mater.* **2020**, *188*, 551–559. [CrossRef]

85. Lee, S.J.; Kim, J.; Kane, S.N.; De Cooman, B.C. On the origin of dynamic strain aging in twinning-induced plasticity steels. *Acta Mater.* **2011**, *59*, 6809–6819. [CrossRef]

86. Kim, J.K.; Chen, L.; Kim, H.S.; Kim, S.K.; Estrin, Y.; De Cooman, B. On the tensile behavior of high-manganese twinning-induced plasticity steel. *Metall. Mater. Trans.* **2009**, *40*, 3147–3158. [CrossRef]

87. Canadinc, D.; Efstathiou, C.; Sehitoglu, H. On the negative strain rate sensitivity of Hadfield steel. *Scr. Mater.* **2008**, *59*, 1103–1106. [CrossRef]

88. Jin, J.E.; Lee, Y.K. Effects of Al on microstructure and tensile properties of C-bearing high Mn TWIP steel. *Acta Mater.* **2012**, *60*, 1680–1688. [CrossRef]

89. Yang, H.; Zhang, Z.; Dong, F.; Duan, Q.; Zhang, Z. Strain rate effects on tensile deformation behaviors for Fe–22Mn–0.6 C–(1.5 Al) twinning-induced plasticity steel. *Mater. Sci. Eng.* **2014**, *607*, 551–558. [CrossRef]

90. Min, J.; Hector Jr, L.G.; Zhang, L.; Sun, L.; Carsley, J.E.; Lin, J. Plastic instability at elevated temperatures in a TRIP-assisted steel. *Mater. Des.* **2016**, *95*, 370–386. [CrossRef]

91. Sevsek, S.; Haase, C.; Bleck, W. Strain-rate-dependent deformation behavior and mechanical properties of a multi-phase medium-manganese steel. *Metals* **2019**, *9*, 344. [CrossRef]

92. Xiong, R.G.; Fu, R.Y.; Yu, S.; Qian, L.; Wei, X.C.; Lin, L. Tensile properties of TWIP steel at high strain rate. *J. Iron Steel Res. Int.* **2009**, *16*, 81–86. [CrossRef]

93. Huang, M.; Yuan, J.; Wang, J.; Wang, L.; Mogucheva, A.; Xu, W. Role of martensitic transformation sequences on deformation-induced martensitic transformation at high strain rates: A quasi in-situ study. *Mater. Sci. Eng.* **2022**, *831*, 142319. [CrossRef]

94. Lambert, P.; Hustedt, C.; Casem, D.; Sinclair, N.; Zhang, X.; Lee, K.; Leong, A.; Schuster, B.; Hufnagel, T. Strain-rate dependence of the martensitic transformation behavior in a 10 Pct Ni multi-phase steel under compression. *Metall. Mater. Trans.* **2020**, *51*, 5101–5109. [CrossRef]

95. Talonen, J.; Hänninen, H.; Nenonen, P.; Pape, G. Effect of strain rate on the strain-induced $\gamma \rightarrow \alpha'$ -martensite transformation and mechanical properties of austenitic stainless steels. *Metall. Mater. Trans.* **2005**, *36*, 421–432. [CrossRef]

96. Liang, Z.Y.; Wang, X.; Huang, W.; Huang, M.X. Strain rate sensitivity and evolution of dislocations and twins in a twinning-induced plasticity steel. *Acta Mater.* **2015**, *88*, 170–179. [CrossRef]

97. Liang, Z.Y.; Huang, W.; Huang, M.X. Suppression of dislocations at high strain rate deformation in a twinning-induced plasticity steel. *Mater. Sci. Eng.* **2015**, *628*, 84–88. [CrossRef]

98. V'azquez-Fern'andez, N.; Isakov, M.; Hokka, M. Strain hardening and adiabatic heating of stainless steels after a sudden increase of strain rate. *J. Dyn. Behav. Mater.* **2022**, *8*, 316–321. [CrossRef]

99. Huang, C.P.; Wang, M.; Zhu, K.Y.; Perlade, A.; Huang, M.X. Carbon-induced negative strain-rate sensitivity in a quenching and partitioning steel. *Acta Mater.* **2023**, *255*, 119099. [CrossRef]